THE JOURNAL OF PHYSICAL CHEMISTRY C
A JOURNAL OF THE AMERICAN CHEMICAL SOCIETY

pubs.acs.org/JPCC
Article

Scanning Tunneling Microscopy Visualization of Polaron Charge Trapping by Hydroxyls on TiO_2(110)

Published as part of The Journal of Physical Chemistry C virtual special issue "Francesc Illas and Gianfranco Pacchioni Festschrift".

Chi-Ming Yim, Michael Allan, Chi Lun Pang, and Geoff Thornton*

Cite This: *J. Phys. Chem. C* 2024, 128, 14100−14106

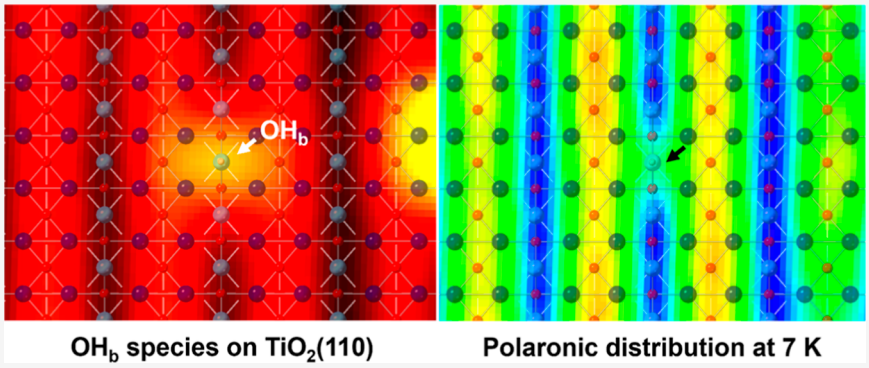

ABSTRACT: Using scanning tunneling microscopy (STM), we investigate the spatial distribution of the bridging hydroxyl (OH_b) bound excess electrons on the rutile TiO_2(110) surface and its temperature dependence. By performing simultaneously recorded empty and filled state imaging on single OH_bs at different temperatures in STM, we determine that the spatial distribution of the OH_b bound excess electrons retains a symmetric four-lobe structure around the OH_b at both 78 and 7 K. This indicates that OH_bs are much weaker charge traps compared to bridging O vacancies (O_b-vac). In addition, by sequentially removing the capping H of each OH_b using voltage pulses, we find that the annihilation of each OH_b is accompanied by the disappearance of some lobes in the filled state STM, thus verifying the direct correlation between OH_bs and their excess electrons.

■ INTRODUCTION

A *Polaron* is a quasiparticle formed when an electronic charge carrier introduced into a dielectric becomes localized at one of the symmetrically equivalent sites available. This alters the equilibrium positions of the surrounding lattice ions and subsequently creates a potential well that traps the carrier.[1]

These self-trapped polarons are believed to play a vital role in the physics and chemistry of many metal oxides, and technologically relevant phenomena as diverse as photolysis,[2] high temperature conductivity[3] and resistive switching.[4] In light of this, polarons in materials including transition metal oxides, cuprates and 2D materials have been extensively characterized,[5−26] and their influence on physical phenomena such as charge transport, surface reactivity and colossal magneto-resistance widely studied.[4,27−35]

Titanium dioxide (TiO_2), a prototypical metal oxide system with applications ranging across heterogeneous catalysis, photolysis and solar cells etc.,[36−40] has recently become a realistic material platform with which to study the polaron properties and their relevance to chemical processes. Taking the most stable (110) face of TiO_2 in the rutile form as an example: its surface structure (Figure 1a) comprises rows of fivefold coordinated Ti^{4+} ions that alternate with those of twofold coordinated bridging O^{2-} ions (O_b).[41] TiO_2 is a wide band-gap insulator (E_{gap} ∼ 3 eV), which can be made semiconducting upon reduction by cycles of ion sputtering and annealing.[42] Such a reduction process leads to the formation of bridging oxygen vacancies (O_b-vacs) on the surface,[43−45] and two excess electrons for each created O_b-vac. Previous studies showed that these excess electrons mainly reside at the subsurface Ti_{6c} sites (beneath the surface Ti_{5c} rows) surrounding the O_b-vacs and reduce the associating Ti

Received: June 5, 2024
Revised: July 28, 2024
Accepted: July 30, 2024
Published: August 8, 2024

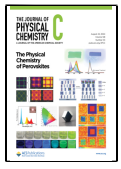

https://doi.org/10.1021/acs.jpcc.4c03751
J. Phys. Chem. C 2024, 128, 14100−14106

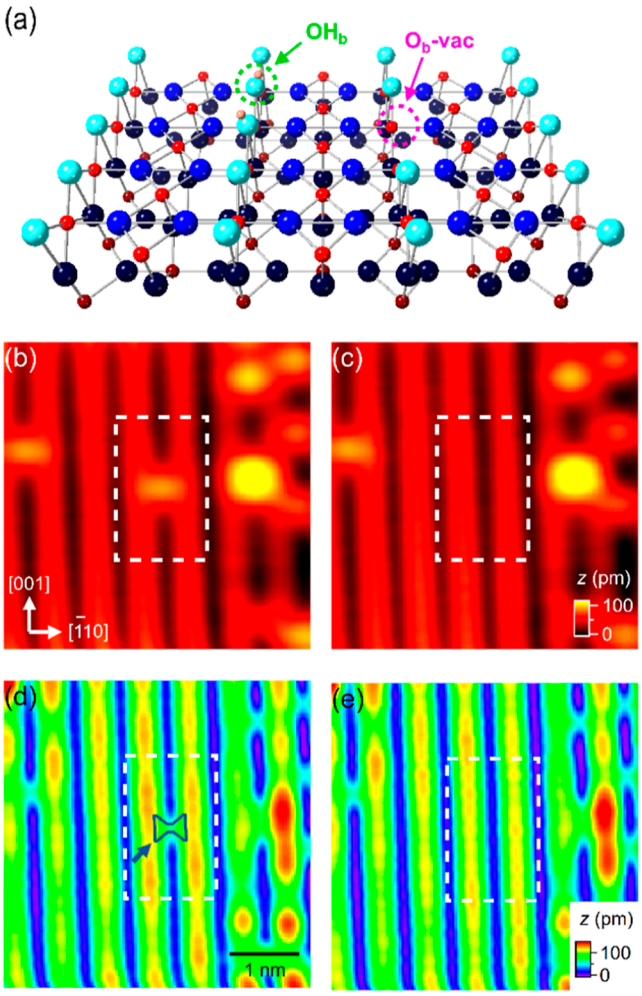

Figure 1. (a) Structural model of rutile $TiO_2(110)$. Spheres of different colors represent O_bs (cyan), in-plane Os (mid blue), subsurface Os (dark blue), surface Ti ions (mid red), sub-surface Ti ions (dark red), and H atoms (pale pink), respectively. O_b-vac and OH_b species are also indicated. (b) Empty- and (d) filled-states 78 K STM images of $(4\ nm)^2$ $TiO_2(110)$ with a single OH_b. In (d), a bow-tie feature at the OH_b site that links the adjacent Ti_{5c} rows is indicated (c,e) As (b,d), recorded after removal of the capping H atom (marked by an arrow) from the OH_b with a 3 V, 1 ms tip pulse. Scan parameters (V, I): (b,d) 0.9 V, 50 pA, and (c,e) −1 V, 50 pA. Dashed rectangles mark the region where the four-lobe excess electron distribution surrounding the OH_b (d) disappears after the capping H removal.

ions,[30,46−49] with a small number occupying the surface Ti sites as observed by resonant photoemission diffraction.[50,51] This results in Ti^{3+} 3d derived defect states, namely the band gap state (BGS), formed at ∼1 eV below the Fermi level (E_F) within the band gap.[52,53] Further studies verified the polaronic character of the O_b-vac bound excess electrons,[54−56] and their strong interaction with adsorbates in model chemical processes.[31,57,58]

O_b-vacs on $TiO_2(110)$ are the most reactive sites for a diverse set of chemical reactions. Taking H_2O adsorption on $TiO_2(110)$ as an example: H_2O molecules adsorb dissociatively at O_b-vacs, forming a pair of bridging hydroxyls (OH_b) for each O_b-vac.[59−63] Over time, the OH_bs within the OH_b pair diffuse away from each other and form two single OH_bs. Previous studies showed that dissociative H_2O adsorption on $TiO_2(110)$ does not cause any change to the BGS population. On this basis, one can assume that upon dissociative H_2O adsorption, the excess electrons originally belonging to O_b-vacs are transferred to the newly formed OH_b pairs, with each pair sharing two excess electrons. Also, it is believed that further splitting of a OH_b pair into two single OH_bs should lead to a redistribution of the excess electrons between the two OH_bs.

Scanning tunneling microscopy (STM), resonant photoemission diffraction, and density functional theory (DFT) calculations have been widely used to study the excess electron distribution in different metal oxide systems owing to their complementary advantages. In particular, using simultaneously recorded empty-(ES) and filled-states (FS) imaging (or dual-mode imaging) in STM, we previously observed that the O_b-vac bound electron polaron distribution adopts a symmetric four-lobe structure surrounding the O_b-vac at 78 K, which transforms into one of the three in-equivalent two-lobe structures as the temperature drops to 7 K.[56] Here, we use low temperature dual-mode imaging in STM to determine how the bound polarons are distributed around the OH_b species following dissociative H_2O adsorption. Moreover, we investigate their temperature dependent behavior. The answers to these questions will further our understanding of the intrinsic difference between O_b-vac and OH_b species as charge traps. It will also illuminate the debate about the difference between the two types of OH_b (one formed at the O_b-vac site and another at one of the neighboring O_b site).[60]

■ EXPERIMENTAL SECTION

STM experiments were performed using an Omicron GmbH low temperature scanning tunneling microscope housed in an ultrahigh vacuum chamber with a base pressure in the 10−11 mbar region. To probe excess electrons associated with OH_b, we performed simultaneously recorded filled (FS, using negative samples bias) and empty states (ES, using positive sample bias) STM imaging (namely, dual-mode imaging): in the forward scan along the fast scan direction, a line of topography data is recorded at positive sample bias; in the backward scan, a line of data is recorded with negative sample bias so that two images (ES and FS images) are recorded quasi-simultaneously. This eliminates the effects of thermal or piezo drift so that images obtained at opposite polarities can be directly correlated. To rule out the possibility of introducing any artifact from the forward scan to the backward scan, the polarity was occasionally reversed, i.e. the forward scans were negatively biased and backward scans were positively biased. No difference was observed in the resulting images.

To obtain a $TiO_2(110)$ single crystal sample with sufficient electrical conductivity for STM measurements at very low temperatures ($T \sim 7$ K), we employed a special sample preparation procedure: first, a fresh rutile $TiO_2(110)$ sample (Pi-Kem) was subjected to about a hundred cycles of argon ion sputtering and vacuum annealing up to 1000 K; then, the as-prepared sample was left in the preparation chamber at a base pressure of 2×10^{-10} mbar at room temperature. In this environment, water from the residual vacuum reacts with O_b-vacs on the sample surface, forming two OH_bs for each O_b-vac.[59−61] In this way, a fully hydroxylated surface (h-TiO_2) with a high density of OH_bs is formed. This reaction removes all the surface O_b-vacs.[64]

We previously showed that the O_b-vac bound polarons separated from each other by at least three unit cells along the [001] direction, or at least one unit cell along [1̄10] have no

https://doi.org/10.1021/acs.jpcc.4c03751
J. Phys. Chem. C 2024, 128, 14100−14106

measurable interaction with each other.[56] On this basis, we prepared single OH_bs on h-TiO_2 as follows: first using dual-mode imaging to locate the OH_bs isolated from regions of charged impurities. Then, using voltage pulses (3 V, 1 ms at 78 K; 3.5 V, 1 ms at 7 K) we removed the capping Hs of all other OH_bs surrounding our targeted OH_b species.[65] This led to a small surface area, usually about (5 nm)-2 containing only a few single noninteracting OH_bs with their associated excess electron distributions.

■ RESULTS AND DISCUSSION

Figure 1 shows a dual-mode 78 K image of a single OH_b on TiO_2(110) (Figure 1b,d), and those taken after the removal of its capping H (Figure 1c,e) using a +3 V, 1 ms tip pulse. Before the capping H removal, the FS image of a single OH_b is characterized by a bowtie-shaped feature at its position linking the neighboring Ti_{5c} rows, altogether with a nearly symmetric four-lobe structure with lobes located at the diagonal Ti_{5c} sites (Figure 1d). All of these features disappear after the capping H is removed (Figure 1e). Previous STM work by Minato et al. observed a similar FS image of single OH_b.[52] Previous DFT calculations of the hydroxylated TiO_2(110) surface show that the Ti_{6c} sites in the second subsurface layer beneath the surface Ti_{5c} rows are the most stable sites for the OH_b-polaron occupation.[46,66] On this basis, we attribute the observed enhanced contrast along the Ti_{5c} rows in the FS images to the excess electrons populating in the second subsurface layer underneath the surface Ti_{5c} rows.

We previously reported that the spatial distribution of the O_b-vac bound excess electrons on the reduced surface of TiO_2(110) (r-TiO_2) transforms from a symmetric four lobe structure at 78 K into one of three asymmetric, two lobe structures at 7 K.[56] Our findings confirmed the polaronic nature of the excess electrons on TiO_2(110), which motivates this study of the spatial distribution of the OH_b bound excess electrons and its temperature dependence. Before looking into this, we first examined how the FS image contrast changes when the capping Hs of a group of OH_bs are removed by using tip pulses. The results are shown in Figure 2, where all of the capping Hs at the center of the imaged region (marked by dashed rectangles) are removed (Figure 2a). In the FS images (Figure 2b), the H-stripped area appears much darker along the Ti_{5c} rows compared with the H-capped region. Hence, there is a direct correlation between OH_bs and the excess electrons that appear as lobes on the Ti_{5c} rows in the FS images (Figure 2b). There are two likely modes in which the excess electrons could dissipate, depending on whether H is desorbed as a cation or a neutral species. In the former, electrons would be lost to the STM apparatus, while in the latter, the electrons would be captured by the bridging O ions.

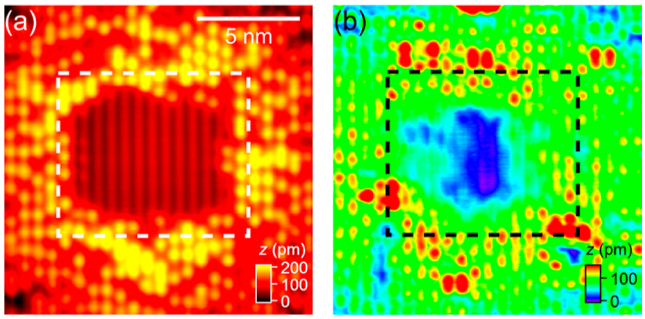

Figure 2. (a) ES- and (b) FS- images of h-TiO_2 recorded after sequential removal of the capping Hs of all OH_bs in the central part of the scanned region using +3.5 V, 1 ms tip pulses. The images were recorded at 7 K. Image size: $(15\ \text{nm})^2$. Scan parameters (V, I): (a) +2 V, 10 pA; (b) −2 V, 1 pA.

Having established the relationship between OH_bs and their associating excess electrons, we turn to the 7 K distribution of excess electrons surrounding single OH_b species. Figure 3 shows the dual-mode images recorded before and after the capping Hs of two single OH_bs was sequentially removed using +3.5 V, 1 ms tip pulses. The ES images in Figure 3a−c simply evidence the conversion of OH_b to O_b. In the FS image (Figure 3d), each OH_b image appears to be characterized by a nearly symmetric four-lobe structure. This is very different from the behavior of O_b-vacs, the excess electron distribution of which is highly asymmetric at 7 K.[56] We attribute this difference to the absence of polaron hopping at low temperature in the case of the O_b-vac bound electrons but not for the OH_b polarons. Intuitively, the much faster hopping of the OH_b bound electrons evidenced at 7 K can be understood by (i) the weaker attractive force of OH_b (formal charge of 1+) to electrons as compared to O_b-vac (formal charge of 2+), and (ii) the much smaller local distortion of the lattice from the formation of an OH_b by adding a H to an O_b as compared to that of O_b-vac (by losing an O_b).

Not only is there little difference between the spatial distribution of the OH_b bound excess electrons at 78 and 7 K, but there is also a similar effect of removing capping H at the two temperatures. Figure 3 shows the dual-mode images of two separated single OH_bs, and those recorded after the sequential removal of their capping Hs by tip pulses. After the capping H on the left is removed (Figure 3b), not only the bowtie-shaped feature in the FS STM at the OH_b center disappears, the lobes distributed at the Ti_{5c} sites around the OH_b (Figure 3d) also vanish in the FS image (Figure 3e). The similar observation also applies to the OH_b on the right (see Figure 3e,f). To better visualize the changes in the FS images, we present in Figure 3g,h, the difference images formed by subtraction of the FS images taken before and after each capping H removal. There, one clearly can see that each OH_b is characterized by a bowtie-shaped feature at the center with four lobes distributed at each of the second nearest Ti_{5c} sites around it. This again confirms the observation of a nearly symmetric, four-lobe structure for the distribution of the OH_b-bound excess electrons at 7 K. Taking a closer look at the difference image (Figure 3g), we also observe a redistribution of the excess electrons in the vicinity of the OH_b on the right after the capping H of the OH_b on the left is removed, as evidenced by the additional lobe of density loss in the bottom region between the two OH_bs. In addition, the difference images (Figure 3g,h) show only a reduction in the FS contrast in close proximity to the OH_bs, while that in the surrounding region remains unchanged. This is consistent with dissipation of the excess electrons through the STM apparatus or capture by bridging O ions, as noted above.

Previous studies showed that when a H_2O molecule adsorbs dissociatively at an O_b-vac, two OH_bs, one at the O_b-vac site (namely v-OH_b) and another at one of the two nearest-neighboring O_b ions (namely b-OH_b), are formed.[59,62] A later STM study by Zhang et al. determined that the capping Hs of b-OH_bs are ten times more likely to hop along the Ti_{5c} rows compared to v-OH_bs, evidencing their inequivalence.[60] One possible scenario is that the distribution of the excess electrons,

https://doi.org/10.1021/acs.jpcc.4c03751
J. Phys. Chem. C 2024, 128, 14100−14106

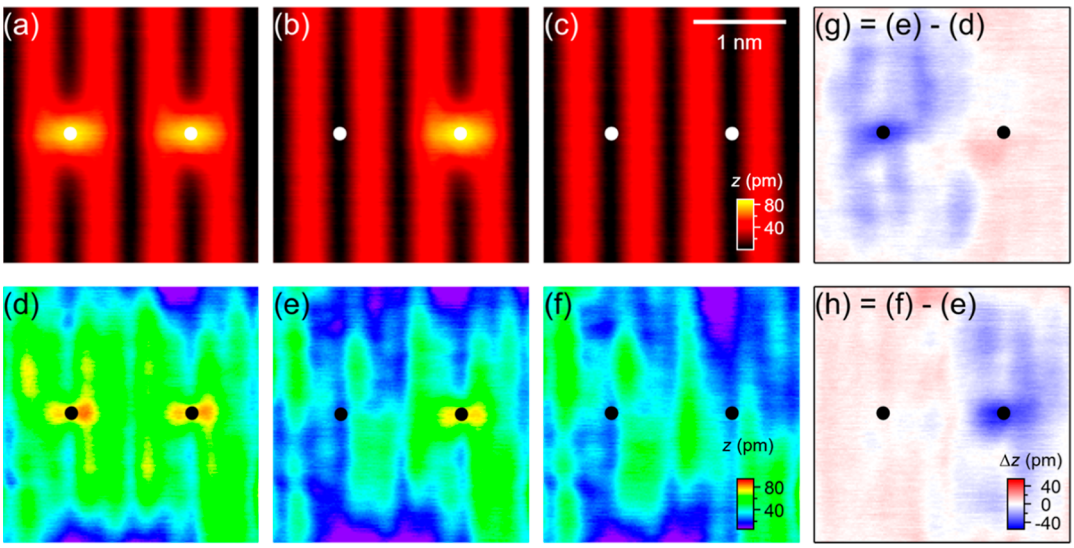

Figure 3. Simultaneously recorded (a) ES and (d) FS images of TiO_2(110) containing two single OH_bs. The images were recorded at 7 K. (b,e) As (a,d) recorded after the capping H of the OH_b on the left was removed by a +3.5 V, 1 ms tip pulse. (c,f) As (b,e) recorded after removal of the capping H of the OH_b on the right. Circles mark the OH_b positions. Image size: $(2.74\ \text{nm})^2$. Scan parameters (V, I): (a−c) +2 V, 30 pA; (d−f) −2 V, 1 pA. (g−h) Difference images formed by subtraction of the FS image in (d) from that in (e), and of the FS image in (e) from that in (f), respectively.

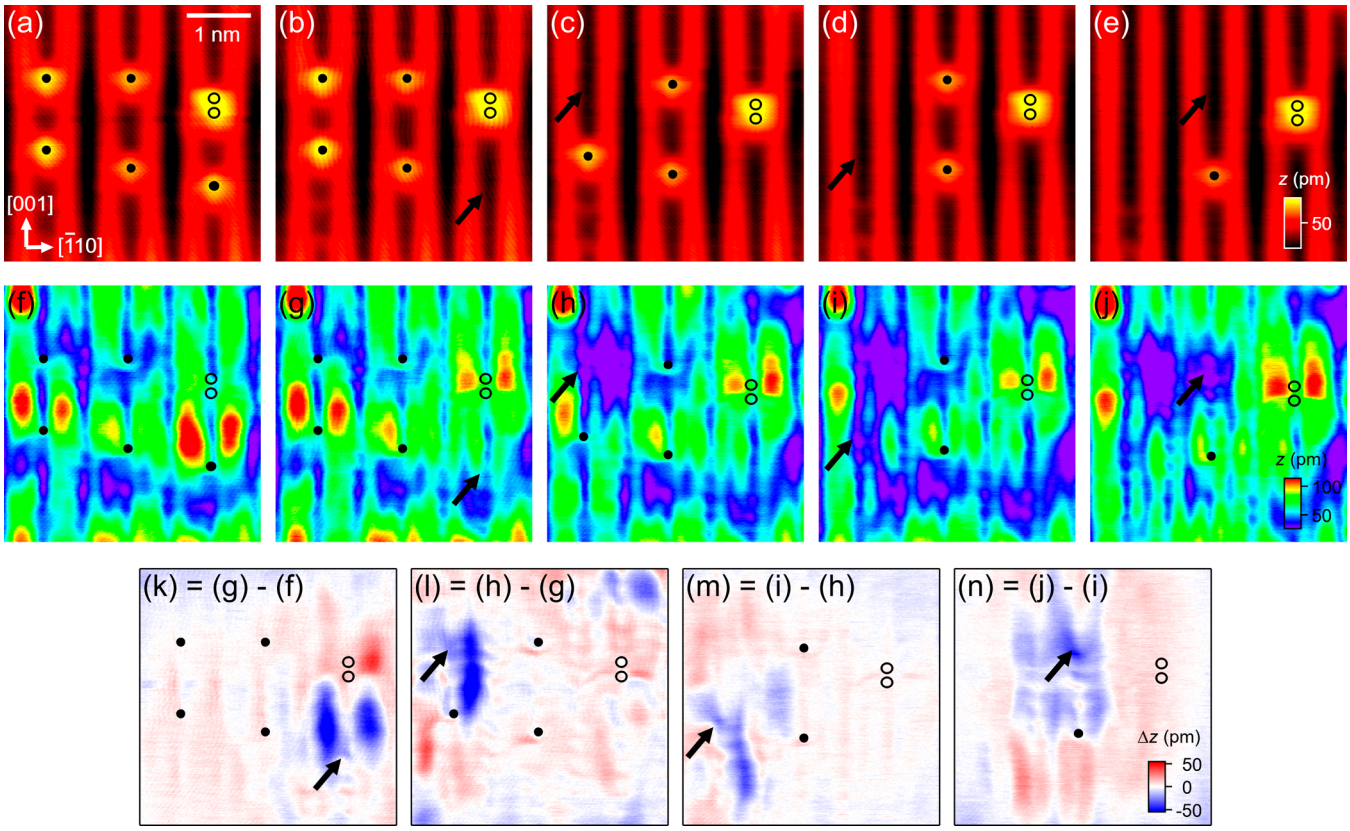

Figure 4. Simultaneously recorded (a) ES and (f) FS images of h-TiO_2. Before imaging, the capping Hs of most OH_bs originally present were removed using +3.5 V, 1 ms tip pulses, leaving only five OH_bs and one OH_b pair remaining in the imaged region. (b−j) As (a−f) following the sequential removal of the capping H of each of the OH_b species using the same tip pulses. Solid circles mark the positions of single OH_bs. Open circles mark those in the OH_b pair. Arrows indicate the capping H being removed in each frame. All images were recorded at 6.6 K. Image size: $(4 \times 4)\ \text{nm}^2$. Scan parameters (V, I): (a−e) +2 V, 30 pA; (f−j) −2 V, 1 pA. (k−n) Difference images formed by subtraction of the FS images obtained before and after the removal of the capping H within each OH_b species.

originally belonging to the O_b-vac, between v- and b-OH_b within a newly formed OH_b pair is uneven. To gain further insight into this, we employed a "pulse and track" approach, i.e. recorded dual-mode STM images before and after each successive removal of the capping Hs from the OH_bs within the OH_b pair using tip pulses. In doing so, we aim to find out

https://doi.org/10.1021/acs.jpcc.4c03751
J. Phys. Chem. C 2024, 128, 14100−14106

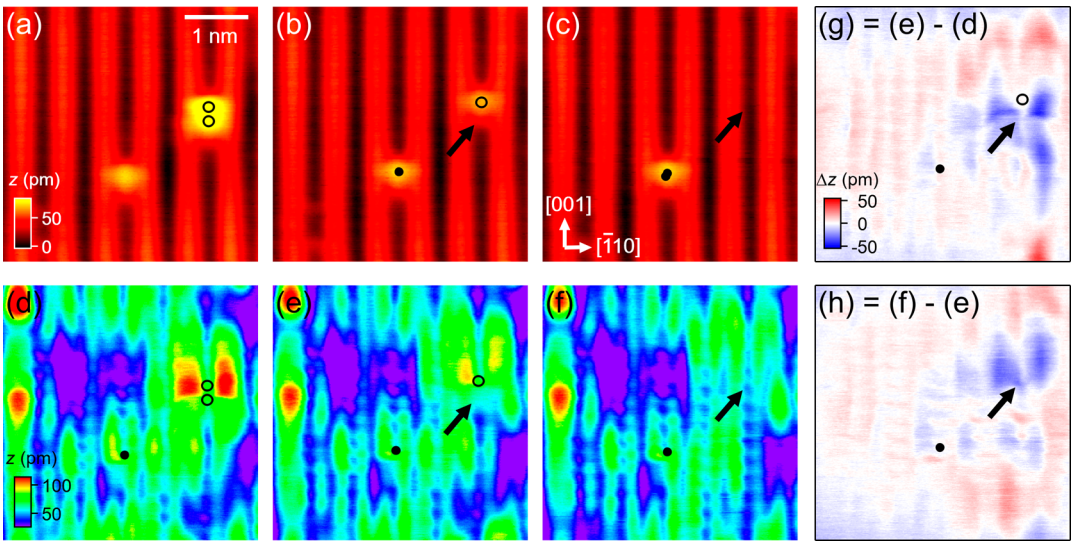

Figure 5. Simultaneously recorded (a) ES and (d) FS images of TiO_2(110) containing one single OH_b and one OH_b pair. (b−c) As (a), but recorded after the capping H atoms of the OH_b pair were removed sequentially using +2.6 V, 200 ms tip pulses. Solid circles mark the positions of single OH_b. Open circles mark the OH_b within the OH_b pair. Arrows indicate the capping H that was removed in each frame. (e−f) Corresponding FS images of (b−c), respectively. All images were recorded at 6.6 K. Image size: (4 × 4) nm^2. Scan parameters (V, I): (a−c) ±2 V, 30 pA; (d−f) −2 V, 1 pA. (g−h) Difference images formed by subtraction of the FS images obtained before and after the removal of each capping H within the OH_b pair.

how the excess electrons are trapped and how they are distributed around each of the OH_bs within the OH_b pair. Before discussing that, we first discuss how successive tip-induced removal of the capping Hs of the OH_b species surrounding a OH_b pair influence the polaron distribution of the OH_b pair.

Figure 4 shows a series of simultaneously recorded dual-mode images, recorded at 6.6 K, taken before and after the sequential removal of each of the capping Hs with tip pulses (+3.5 V, 1 ms). Before imaging, the capping Hs of most of the OH_bs originally present in the scanned region were removed using the same tip pulses. This leaves only five OH_bs and one OH_b pair remaining in the scanned region. As shown in the FS images (Figure 4f−j) and in the difference images (Figure 4k−n), the removal of each capping H is always accompanied by changes in image contrast in the FS image. Taking the OH_b at the bottom right as an example, after its capping H is removed (Figure 4b), the two lobes originally present at the Ti_{5c} sites above that of OH_b disappear (Figure 4f). Their disappearance is also accompanied by some increase in the intensity of the lobes at the Ti sites above the OH_b pair at the top right of the image (Figure 4g). This indicates that not only does the removal of that capping H lead to a dissipation of the associated excess electrons but also it results in modification of the excess electron distribution surrounding that OH_b-pair. Similar changes to the excess electron distributions surrounding the OH_b and OH_b pair on the surface have also been observed following the removal of other capping Hs, see the images (Figure 4g−j) and the corresponding difference images (Figure 4l−n) for such changes.

In addition to studying the influence of neighboring OH_bs on the polaron distribution surrounding a OH_b pair, we have also investigated how the polaron distribution surrounding an OH_b pair changes upon the sequential removal of its capping Hs, and our results are shown in Figure 5. The initial empty and filled state images are shown in Figure 5a,d, respectively. The filled state image evidences a distribution of the OH_b pair bound polarons that has a three lobe structure. The apparent asymmetry in the FS image is consistent with the asymmetric behavior observed by Zhang *et al.* in the mobility of the two types of bridging hydroxyls.[60] After the first capping H within the OH_b pair was removed by a tip pulse (Figure 5b), the lobes become significantly weaker in intensity and displace away from their original positions (Figure 5e,g). Then, after the second capping H was removed (Figure 5c), the lobes further weaken and dissipate further away from the original position of the OH_b pair (Figure 5f,h). Based on the above, we conclude that, first, OH_bs are weaker as charge traps compared to a OH_b pair, and second, as all the charge traps on the surface are removed, the excess electrons originally bound to those charge traps are dissipated. Meanwhile, the resulting absence of any charge traps leads to much more uniform appearance along the Ti_{5c} rows (Figure 5f).

Through comparison of the STM data shown in Figures 3−5, we find that the almost symmetric four-lobe structure of the spatial distribution of the OH_b bound polarons at T = 7 K transforms into one of the asymmetric two- or three-lobe structures as temperature is reduced to 6.6 K. We attribute such change in the polaronic distribution to the temperature-dependent hopping behavior of polarons: at 7 K polarons still hop between the subsurface Ti_{6c} sites surrounding a OH_b and their motion starts to freeze; at 6.6 K their motion becomes completely frozen and depending on the local chemical environment,[56] their distribution about a OH_b adopts one of the asymmetric structures.

■ SUMMARY

To summarize, employing dual-mode imaging to study the spatial distribution of the OH_b bound excess electrons on the (110) surface of TiO_2 rutile, we found that their distributions retain a symmetric, four-lobe structure at temperature of 7 K, suggesting that OH_bs are much weaker as charge traps compared to O_b-vacs, with their associated polarons requiring much less energy to hop over different Ti sites surrounding the

https://doi.org/10.1021/acs.jpcc.4c03751
J. Phys. Chem. C 2024, 128, 14100−14106

vacancies. In addition, using voltage pulses to sequentially remove the capping H of each of the OH_bs and monitoring the corresponding changes in the image contrast within the FS STM, we found that every capping H removal is accompanied by the disappearance of some FS contrast surrounding the removed capping H position, thus verifying that each OH_b, once formed, is accompanied by a polaron.

■ AUTHOR INFORMATION

Corresponding Author

Geoff Thornton − *Department of Chemistry and London Centre for Nanotechnology, University College London, London WC1H 0AJ, U.K.;* orcid.org/0000-0002-1616-5606; Email: g.thornton@ucl.ac.uk

Authors

Chi-Ming Yim − *Department of Chemistry and London Centre for Nanotechnology, University College London, London WC1H 0AJ, U.K.; Tsung Dao Lee Institute and School of Physics and Astronomy, Shanghai Jiao Tong University, Shanghai 201210, China;* orcid.org/0000-0003-3339-4571

Michael Allan − *Department of Chemistry and London Centre for Nanotechnology, University College London, London WC1H 0AJ, U.K.*

Chi Lun Pang − *Department of Chemistry and London Centre for Nanotechnology, University College London, London WC1H 0AJ, U.K.;* orcid.org/0000-0002-5222-9734

Complete contact information is available at: https://pubs.acs.org/10.1021/acs.jpcc.4c03751

Notes

The authors declare no competing financial interest.

■ ACKNOWLEDGMENTS

We are grateful to Matthew Wolf for useful discussions. This work was supported by the European Research Council Advanced Grant ENERGYSURF (G.T.), the EPSRC through grant EP/L015277/1, European Cooperation in Science and Technology Action CM1104, the Royal Society (UK), and Alexander von Humboldt Stiftung (Germany). C.M.Y. acknowledges support from a TDLI Start-up fund.

■ REFERENCES

(1) Emin, D. *Polarons*; Cambridge University Press: Cambridge, 2012.

(2) *Metal Oxide Catalysis*; Jackson, S. D., Hargreaves, J. S. J., Eds.; Wiley VCH: Weinheim, 2009; .

(3) *Polarons and Bipolarons in High-Tc Superconductors and Related Materials*; Salje, E. K. H., Alexandrov, A. S., Liang, W. Y., Eds.; Cambridge University Press: Cambridge, 1995; .

(4) Wang, M.; Bi, C.; Li, L.; Long, S.; Liu, Q.; Lv, H.; Lu, N.; Sun, P.; Liu, M. Thermoelectric Seebeck effect in oxide-based resistive switching memory. *Nat. Commun.* **2014**, *5*, 4598.

(5) *Polarons in Advanced Materials*; Alexandrov, A. S., Ed. ; *Springer Series in Materials Science*; Springer: Dordrecht, 2007; Vol. *103*

(6) Nagels, P.; Denayer, M.; Devreese, J. Electrical properties of single crystals of uranium dioxide. *Solid State Commun.* **1963**, *1*, 35−40.

(7) Crevecoeur, C.; De Wit, H. Electrical conductivity of Li doped MnO. *J. Phys. Chem. Solids* **1970**, *31*, 783−791.

(8) Stoneham, A. M.; Gavartin, J.; Shluger, A. L.; Kimmel, A. V.; Ramo, D. M.; Rønnow, H. M.; Aeppli, G.; Renner, C. Trapping, self-trapping and the polaron family. *J. Phys.: Condens. Matter* **2007**, *19*, 255208.

(9) Coropceanu, V.; Cornil, J.; da Silva Filho, D. A.; Olivier, Y.; Silbey, R.; Brédas, J. L. Charge Transport in Organic Semiconductors. *Chem. Rev.* **2007**, *107*, 926−952.

(10) Zhugayevych, A.; Tretiak, S. Theoretical Description of Structural and Electronic Properties of Organic Photovoltaic Materials. *Annu. Rev. Phys. Chem.* **2015**, *66*, 305−330.

(11) De Sio, A.; Troiani, F.; Maiuri, M.; Réhault, J.; Sommer, E.; Lim, J.; Huelga, S. F.; Plenio, M. B.; Rozzi, C. A.; Cerullo, G.; et al. Tracking the coherent generation of polaron pairs in conjugated polymers. *Nat. Commun.* **2016**, *7*, 13742.

(12) Kaminski, A.; Das Sarma, S. Polaron Percolation in Diluted Magnetic Semiconductors. *Phys. Rev. Lett.* **2002**, *88*, 247202.

(13) Teresa, J. M. D.; Ibarra, M. R.; Algarabel, P. A.; Ritter, C.; Marquina, C.; Blasco, J.; García, J.; del Moral, A.; Arnold, Z. Evidence for magnetic polarons in the magneto-resistive perovskites. *Nature* **1997**, *386*, 256−259.

(14) Zhou, J.-S.; Goodenough, J. B. Zener versus de Gennes ferromagnetism in $La_{1-x}Sr_xMnO_3$. *Phys. Rev. B* **2000**, *62*, 3834−3838.

(15) Daoud-Aladine, A.; Rodríguez-Carvajal, J.; Pinsard-Gaudart, L.; Fernández-Díaz, M. T.; Revcolevschi, A. Zener Polaron Ordering in Half-Doped Manganites. *Phys. Rev. Lett.* **2002**, *89*, 097205.

(16) Yamada, Y.; Hino, O.; Nohdo, S.; Kanao, R.; Inami, T.; Katano, S. Polaron Ordering in Low-Doping $La_{1-x}Sr_xMnO_3$. *Phys. Rev. Lett.* **1996**, *77*, 904−907.

(17) Zhao, G.-M.; Hunt, M. B.; Keller, H.; Müller, K. A. Evidence for polaronic supercarriers in the copper oxide superconductors $La_{2-x}Sr_xCuO_4$. *Nature* **1997**, *385*, 236−239.

(18) Cortecchia, D.; Yin, J.; Bruno, A.; Lo, S.-Z. A.; Gurzadyan, G. G.; Mhaisalkar, S.; Brédas, J. L.; Soci, C. Polaron self-localization in white-light emitting hybrid per- ovskites. *J. Mater. Chem. C* **2017**, *5*, 2771−2780.

(19) Miyata, K.; Meggiolaro, D.; Trinh, M. T.; Joshi, P. P.; Mosconi, E.; Jones, S. C.; De Angelis, F.; Zhu, X.-Y. Large polarons in lead halide perovskites. *Sci. Adv.* **2017**, *3*, No. e1701217.

(20) Chen, Q.; Wang, W.; Peeters, F. M. Magneto-polarons in monolayer transition-metal dichalcogenides. *J. Appl. Phys.* **2018**, *123*, 214303.

(21) Kang, M.; Jung, S. W.; Shin, W. J.; Sohn, Y.; Ryu, S. H.; Kim, T. K.; Hoesch, M.; Kim, K. S. Holstein polaron in a valley-degenerate two-dimensional semiconductor. *Nat. Mater.* **2018**, *17*, 676−680.

(22) McKenna, K. P.; Wolf, M. J.; Shluger, A. L.; Lany, S.; Zunger, A. Two-Dimensional Polaronic Behavior in the Binary Oxides m-HfO_2 and m-ZrO_2. *Phys. Rev. Lett.* **2012**, *108*, 116403.

(23) Reticcioli, M.; Wang, Z.; Schmid, M.; Wrana, D.; Boatner, L. A.; Diebold, U.; Setvin, M.; Franchini, C. Competing electronic states emerging on polar surfaces. *Nat. Commun.* **2022**, *13*, 4311.

(24) Liu, H.; Wang, A.; Zhang, P.; Ma, C.; Chen, C.; Liu, Z.; Zhang, Y.-Q.; Feng, B.; Cheng, P.; Zhao, J.; et al. Atomic-scale manipulation of single-polaron in a two-dimensional semiconductor. *Nat. Commun.* **2023**, *14*, 3690.

(25) Cai, M.; Miao, M.-P.; Liang, Y.; Jiang, Z.; Liu, Z.-Y.; Zhang, W.-H.; Liao, X.; Zhu, L.-F.; West, D.; Zhang, S.; et al. Manipulating single excess electrons in monolayer transition metal dihalide. *Nat. Commun.* **2023**, *14*, 3691.

(26) Yue, X.; Wang, C.; Zhang, B.; Zhang, Z.; Xiong, Z.; Zu, X.; Liu, Z.; Hu, Z.; Odunm-baku, G. O.; Zheng, Y.; et al. Real-time observation of the buildup of polaron in α-$FAPbI_3$. *Nat. Commun.* **2023**, *14*, 917.

(27) Nelson, J.; Kwiatkowski, J. J.; Kirkpatrick, J.; Frost, J. M. Modeling Charge Transport in Organic Photovoltaic Materials. *Acc. Chem. Res.* **2009**, *42*, 1768−1778.

(28) Ortmann, F.; Bechstedt, F.; Hannewald, K. Charge transport in organic crystals: Theory and modelling. *Phys. Status Solidi B* **2011**, *248*, 511−525.

(29) Di Valentin, C.; Pacchioni, G.; Selloni, A. Reduced and n-Type Doped TiO_2: Nature of Ti^{3+}*Species*. *J. Phys. Chem. C* **2009**, *113*, 20543−20552.

(30) Papageorgiou, A. C.; Beglitis, N. S.; Pang, C. L.; Teobaldi, G.; Cabailh, G.; Chen, Q.; Fisher, A. J.; Hofer, W. A.; Thornton, G. Electron traps and their effect on the surface chemistry of TiO_2(110). *Proc. Natl. Acad. Sci. USA* **2010**, *107*, 2391−2396.
(31) Reticcioli, M.; Sokolović, I.; Schmid, M.; Diebold, U.; Setvin, M.; Franchini, C. Interplay between Adsorbates and Polarons: CO on Rutile TiO_2(110). *Phys. Rev. Lett.* **2019**, *122*, 016805.
(32) Yin, W.-J.; Wen, B.; Zhou, C.; Selloni, A.; Liu, L.-M. Excess electrons in reduced rutile and anatase TiO_2. *Surf. Sci. Rep.* **2018**, *73*, 58−82.
(33) Reticcioli, M.; Setvin, M.; Hao, X.; Flauger, P.; Kresse, G.; Schmid, M.; Diebold, U.; Franchini, C. Polaron-Driven Surface Reconstructions. *Phys. Rev. X* **2017**, *7*, 031053.
(34) Millis, A. J.; Mueller, R.; Shraiman, B. I. Fermi-liquid-to-polaron crossover. II. Double exchange and the physics of colossal magnetoresistance. *Phys. Rev. B* **1996**, *54*, 5405−5417.
(35) Verdi, C.; Caruso, F.; Giustino, F. Origin of the crossover from polarons to Fermi liquids in transition metal oxides. *Nat. Commun.* **2017**, *8*, 15769.
(36) Imagawa, H.; Tanaka, T.; Takahashi, N.; Matsunaga, S.; Suda, A.; Shinjoh, H. Synthesis and characterization of Al_2O_3 and ZrO_2−TiO_2 nano-composite as a support for NOx storage−reduction catalyst. *J. Catal.* **2007**, *251*, 315−320.
(37) Fujishima, A.; Honda, K. Electrochemical Photolysis of Water at a Semiconductor Electrode. *Nature* **1972**, *238*, 37−38.
(38) O'Regan, B.; Grätzel, M. A low-cost, high-efficiency solar cell based on dye-sensitized colloidal TiO_2 films. *Nature* **1991**, *353*, 737−740.
(39) Grätzel, M. Photoelectrochemical cells. *Nature* **2001**, *414*, 338−344.
(40) Majumder, D.; Roy, S. Room Temperature Synthesis of TiO_2 Nanospheres: Ammonia Sensing Characteristics. *Mater. Today: Proc.* **2018**, *5*, 9811−9816.
(41) Pang, C. L.; Lindsay, R.; Thornton, G. Chemical reactions on rutile TiO_2(110). *Chem. Soc. Rev.* **2008**, *37*, 2328−2353.
(42) Diebold, U. The surface science of titanium dioxide. *Surf. Sci. Rep.* **2003**, *48*, 53−229.
(43) Hugenschmidt, M. B.; Gamble, L.; Campbell, C. T. The interaction of H_2O with a TiO_2(110) surface. *Surf. Sci.* **1994**, *302*, 329−340.
(44) Henderson, M. A. Structural Sensitivity in the Dissociation of Water on TiO_2 Single- Crystal Surfaces. *Langmuir* **1996**, *12*, 5093−5098.
(45) Henderson, M. A. A surface perspective on self-diffusion in rutile TiO_2. *Surf. Sci.* **1999**, *419*, 174−187.
(46) Deskins, N. A.; Rousseau, R.; Dupuis, M. Localized Electronic States from Surface Hydroxyls and Polarons in TiO_2(110). *J. Phys. Chem. C* **2009**, *113*, 14583−14586.
(47) Deskins, N. A.; Rousseau, R.; Dupuis, M. Distribution of Ti^{3+} Surface Sites in Reduced TiO_2. *J. Phys. Chem. C* **2011**, *115*, 7562−7572.
(48) Kowalski, P. M.; Camellone, M. F.; Nair, N. N.; Meyer, B.; Marx, D. Charge Localization Dynamics Induced by Oxygen Vacancies on the TiO_2(110) Surface. *Phys. Rev. Lett.* **2010**, *105*, 146405.
(49) Reticcioli, M.; Setvin, M.; Schmid, M.; Diebold, U.; Franchini, C. Formation and dynamics of small polarons on the rutile TiO_2(110) surface. *Phys. Rev. B* **2018**, *98*, 045306.
(50) Krüger, P.; Bourgeois, S.; Domenichini, B.; Magnan, H.; Chandesris, D.; Le Fèvre, P.; Flank, A. M.; Jupille, J.; Floreano, L.; Cossaro, A.; et al. Defect States at the TiO_2(110) Surface Probed by Resonant Photoelectron Diffraction. *Phys. Rev. Lett.* **2008**, *100*, 055501.
(51) Krüger, P.; Jupille, J.; Bourgeois, S.; Domenichini, B.; Verdini, A.; Floreano, L.; Morgante, A. Intrinsic Nature of the Excess Electron Distribution at the TiO_2(110) Surface. *Phys. Rev. Lett.* **2012**, *108*, 126803.
(52) Minato, T.; Sainoo, Y.; Kim, Y.; Kato, H. S.; Aika, K.-i.; Kawai, M.; Zhao, J.; Petek, H.; Huang, T.; He, W.; et al. The electronic structure of oxygen atom vacancy and hydroxyl impurity defects on titanium dioxide (110) surface. *J. Chem. Phys.* **2009**, *130*, 124502.
(53) Yim, C. M.; Pang, C. L.; Thornton, G. Oxygen Vacancy Origin of the Surface Band-Gap State of TiO_2(110). *Phys. Rev. Lett.* **2010**, *104*, 036806.
(54) Sezen, H.; Buchholz, M.; Nefedov, A.; Natzeck, C.; Heissler, S.; Di Valentin, C.; Wöll, C. Probing electrons in TiO_2 polaronic trap states by IR-absorption: Evidence for the existence of hydrogenic states. *Sci. Rep.* **2014**, *4*, 3808.
(55) Setvin, M.; Franchini, C.; Hao, X.; Schmid, M.; Janotti, A.; Kaltak, M.; Van de Walle, C. G.; Kresse, G.; Diebold, U. Direct View at Excess Electrons in TiO_2 Rutile and Anatase. *Phys. Rev. Lett.* **2014**, *113*, 086402.
(56) Yim, C.; Watkins, M.; Wolf, M.; Pang, C.; Hermansson, K.; Thornton, G. Engineering Polarons at a Metal Oxide Surface. *Phys. Rev. Lett.* **2016**, *117*, 116402.
(57) Yim, C. M.; Chen, J.; Zhang, Y.; Shaw, B.-J.; Pang, C. L.; Grinter, D. C.; Bluhm, H.; Salmeron, M.; Muryn, C. A.; Michaelides, A.; et al. Visualization of Water- Induced Surface Segregation of Polarons on Rutile TiO_2(110). *J. Phys. Chem. Lett.* **2018**, *9*, 4865−4871.
(58) Gao, C.; Zhang, L.; Zheng, Q.; Zhao, J. Tuning the Lifetime of Photoexcited Small Polarons on Rutile TiO_2 Surface via Molecular Adsorption. *J. Phys. Chem. C* **2021**, *125*, 27275−27282.
(59) Bikondoa, O.; Pang, C. L.; Ithnin, R.; Muryn, C. A.; Onishi, H.; Thornton, G. Direct visualization of defect-mediated dissociation of water on TiO_2(110). *Nat. Mater.* **2006**, *5*, 189−192.
(60) Zhang, Z.; Bondarchuk, O.; Kay, B. D.; White, J. M.; Dohnálek, Z. Imaging Water Dissociation on TiO_2(110): Evidence for Inequivalent Geminate OH Groups. *J. Phys. Chem. B* **2006**, *110*, 21840−21845.
(61) Wendt, S.; Schaub, R.; Matthiesen, J.; Vestergaard, E.; Wahlström, E.; Rasmussen, M.; Thostrup, P.; Molina, L.; Lægsgaard, E.; Stensgaard, I.; et al. Oxygen vacancies on TiO_2(110) and their interaction with H_2O and O_2: A combined high-resolution STM and DFT study. *Surf. Sci.* **2005**, *598*, 226−245.
(62) Wendt, S.; Matthiesen, J.; Schaub, R.; Vestergaard, E. K.; Lægsgaard, E.; Besen-bacher, F.; Hammer, B. Formation and Splitting of Paired Hydroxyl Groups on Reduced TiO_2(110). *Phys. Rev. Lett.* **2006**, *96*, 066107.
(63) Brookes, I. M.; Muryn, C. A.; Thornton, G. Imaging Water Dissociation on TiO_2(110). *Phys. Rev. Lett.* **2001**, *87*, 266103.
(64) Matthey, D.; Wang, J. G.; Wendt, S.; Matthiesen, J.; Schaub, R.; Lægsgaard, E.; Hammer, B.; Besenbacher, F. Enhanced Bonding of Gold Nanoparticles on Oxidized TiO_2(110). *Science* **2007**, *315*, 1692−1696.
(65) Minato, T.; Kajita, S.; Pang, C.-L.; Asao, N.; Yamamoto, Y.; Nakayama, T.; Kawai, M.; Kim, Y. Tunneling Desorption of Single Hydrogen on the Surface of Titanium Dioxide. *ACS Nano* **2015**, *9*, 6837−6842.
(66) Deskins, N. A.; Dupuis, M. Electron transport via polaron hopping in bulk TiO_2: A density functional theory characterization. *Phys. Rev. B* **2007**, *75*, 195212.

https://doi.org/10.1021/acs.jpcc.4c03751
J. Phys. Chem. C 2024, 128, 14100−14106